J Mol Model (2008) 14:621–630
DOI 10.1007/s00894-008-0316-x

ORIGINAL PAPER

Modeling of hydrogen-assisted cracking in iron crystal using a quasi-Newton method

Igor Ye. Telitchev · Oleg Vinogradov

Received: 2 November 2007 / Accepted: 14 April 2008 / Published online: 15 May 2008

Abstract A Quasi-Newton method was applied in the context of a molecular statics approach to simulate the phenomenon of hydrogen embrittlement of an iron lattice. The atomic system is treated as a truss-type structure. The interatomic forces between the hydrogen–iron and the iron–iron atoms are defined by Morse and modified Morse potential functions, respectively. Two-dimensional hexagonal and 3D bcc crystal structures were subjected to tensile numerical tests. It was shown that the Inverse Broyden's Algorithm—a quasi-Newton method—provides a computationally efficient technique for modeling of the hydrogen-assisted cracking in iron crystal. Simulation results demonstrate that atoms of hydrogen placed near the crack tip produce a strong deformation and crack propagation effect in iron lattice, leading to a decrease in the residual strength of numerically tested samples.

Keywords Atomistic simulation · Molecular statics · Hydrogen-assisted cracking

Introduction

Hydrogen embrittlement is one of the most dangerous phenomena affecting the mechanical properties of commercial steel. Hydrogen is highly mobile and can diffuse through the crystal lattice, dissolving into its interstitial sites [1, 2]. The presence of stress in a metal significantly intensifies the process of hydrogen absorption; hydrogen accumulates in the immediate vicinity ahead of the crack tip and it can contribute to catastrophic failures [3] even without significant deformation of the material structure. The oil and gas markets are challenged by the growing demand for ever-increasing strength in pipelines for the transportation of gas or petrochemical products. Since high strength steels are more vulnerable to the presence of hydrogen [4], their use makes hydrogen embrittlement a continuing concern in the oil and gas industries.

Despite extensive studies, the mechanisms of hydrogen effects on subcritical crack nucleation and growth have remained unclear due to a number of factors governing it on the atomic level. Since experimental studies cannot usually reach the atomic scale, analysis at the atomistic level offers an opportunity to investigate the nature of hydrogen embrittlement.

A number of atomistic simulations on the effect of hydrogen have been performed for single iron crystals in the past [5–12]. Among the most important results was evidence for a phenomenon that became known as embrittlement. However, these results were mostly qualitative and did not include the deformation characteristics of the embrittled iron crystal, which are the basis for a comprehensive understanding of hydrogen embrittlement mechanisms. In the following, in order to provide deeper insights into the phenomenon of embrittlement, the influence of hydrogen is simulated by using the quasi-Newton method in numerical nano-scale tensile tests on hydrogen-saturated iron crystal.

I. Y. Telitchev (✉) · O. Vinogradov
Department of Mechanical and Manufacturing Engineering,
University of Calgary,
2500 University Drive NW,
Calgary, AB T2N 1N4, Canada
e-mail: iytelitc@ucalgary.ca

Methods

Choice of atomistic method for modeling

Atomic-scale modeling of the fracture behavior of materials belongs to the current challenges of materials science. Atomistic simulation methods based on classical force fields provide a computationally efficient means of atomistic simulation of nano-scale deformation and fracture. These methods include molecular dynamics (MD) and molecular statics (MS) techniques.

In problems dealing with crack formation, the time-independent MS approach is widely used [13–17]. A limitation of this approach is that the simulation is performed for a 0°K temperature, but it has the advantage that it allows the dynamic process of cracking to be followed in a quasistatic manner, which in MD would be possible only by extraordinarily long time trajectories. The analysis presented in this paper falls into the MS formulation framework.

Within the MS framework there are two different approaches that provide ways of finding the equilibrium position of the atomic structure. The equilibrium position can be reached by either minimizing the total system potential energy or by moving the atoms until the maximum net force on any atom becomes sufficiently small. The choice of boundary conditions defines the type of numerical algorithm to be applied for the calculation.

Two major families of algorithms are most appropriate for finding the equilibrium position of atomic systems subjected to boundary displacements. The first family goes under the name "conjugate gradient methods" and the second, "quasi-Newton methods". As illustrated in Table 1, the estimated number of arithmetic operations for both approaches is $\boldsymbol{O}(N^2)$ [18–20]. In the case of stress boundary conditions, the Newton-Raphson and the quasi-Newton methods are most frequently used. Note, however, that the Newton-Raphson method is computationally demanding, requiring $\boldsymbol{O}(N^3)$ arithmetic operations, and, in this respect, the quasi-Newton method is superior.

Of the aforementioned algorithms, the conjugate gradient method and the quasi-Newton method require the least possible number of arithmetic operations, namely $\boldsymbol{O}(N^2)$.

Table 1 Choice of simulation method

Most appropriate method	Boundary conditions		Number of arithmetic operations
	Boundary displacement	Applied stress	
Conjugate gradient	X		$O(N^2)$
Quasi-Newton	X	X	$O(N^2)$
Newton–Raphson		X	$O(N^3)$

While the conjugate gradient and quasi-Newton methods are similar in terms of their computational efficiency, application of the former is restricted to displacement boundary conditions, while the quasi-Newton method does not have such a limitation and can be applied not only to boundary displacement but also to force or mixed boundary conditions. Both these advantages—computational efficiency and universality—make the quasi-Newton method attractive for implementation in atomistic-scale modeling of material deformation and fracture.

Simulation techniques

From the structural point of view, material degradation constitutes the re-arrangement of atomic positions and transformation of the lattice as a structure. The proposed time-independent quasi-static approach is based on integration of MS and structural mechanics approaches. Following this approach, the crystal structure is treated as a truss system, with the forces between the atoms situated at the nodes defined by inter-atomic potentials. According to the Morse function, the potential energy of two atoms i and j separated by a distance R_{ij} is defined as follows:

$$\Phi(\mathrm{x})=\varepsilon\left(\mathrm{e}^{-2\mathrm{m}(\mathrm{x}-1)}-2\mathrm{e}^{-\mathrm{m}(\mathrm{x}-1)}\right) \tag{1}$$

where $\mathrm{x}=\mathrm{R_{ij}}/\mathrm{R_e}$ is the interatomic distance (dimensionless), R_{ij} the interatomic distance (Å), R_e the equilibrium distance (Å), and ε and m are constants.

The Morse potential function developed by Olander, and the modified Morse potential developed by Fujiwara and Ishii were used to describe the H–Fe and the Fe–Fe interatomic interactions, respectively [9, 21]. The analysis presented in [12] showed that these potentials "agree fairly well with experimental values".

The following Morse potential parameters were used:

1. H–Fe potential: a=2. 2.867 [(Å); R_e=1.12a (Å); m=2.96; ε=4.6 kcal mol^{-1} [21]
2. Fe–Fe potential: a=2.867 (Å) R_e=0.993a (Å); m=3.95; ε=9.63 kcal mol^{-1} [21, 22]

In the modified Morse potential of Fe–Fe, the long-range tail of the original Morse potential was truncated by using a function $f(x)$. Thus, the modified Morse potential takes the form:

$$\Phi_{\mathrm{Modified}}(\mathrm{x})=\Phi(\mathrm{x})\cdot\mathrm{f}(\mathrm{x}), \tag{2}$$

where

$$f(x)=\begin{cases}1 & x<1\\ 3z^4-8z^3+6z^2 & x_c>x>1\\ 0 & x>x_c\end{cases} \tag{3}$$

$\mathrm{z}=(\mathrm{x}-\mathrm{x_c})/(1-\mathrm{x_c})$; $\mathrm{x_c}=\mathrm{R_{cut-off}}/\mathrm{R_e}$. According to Fujiwara-Ishii [21], x_c=1.4. So ,at this distance ($R_{cut\text{-}off}/R_e$=1.4) ,the Fe–

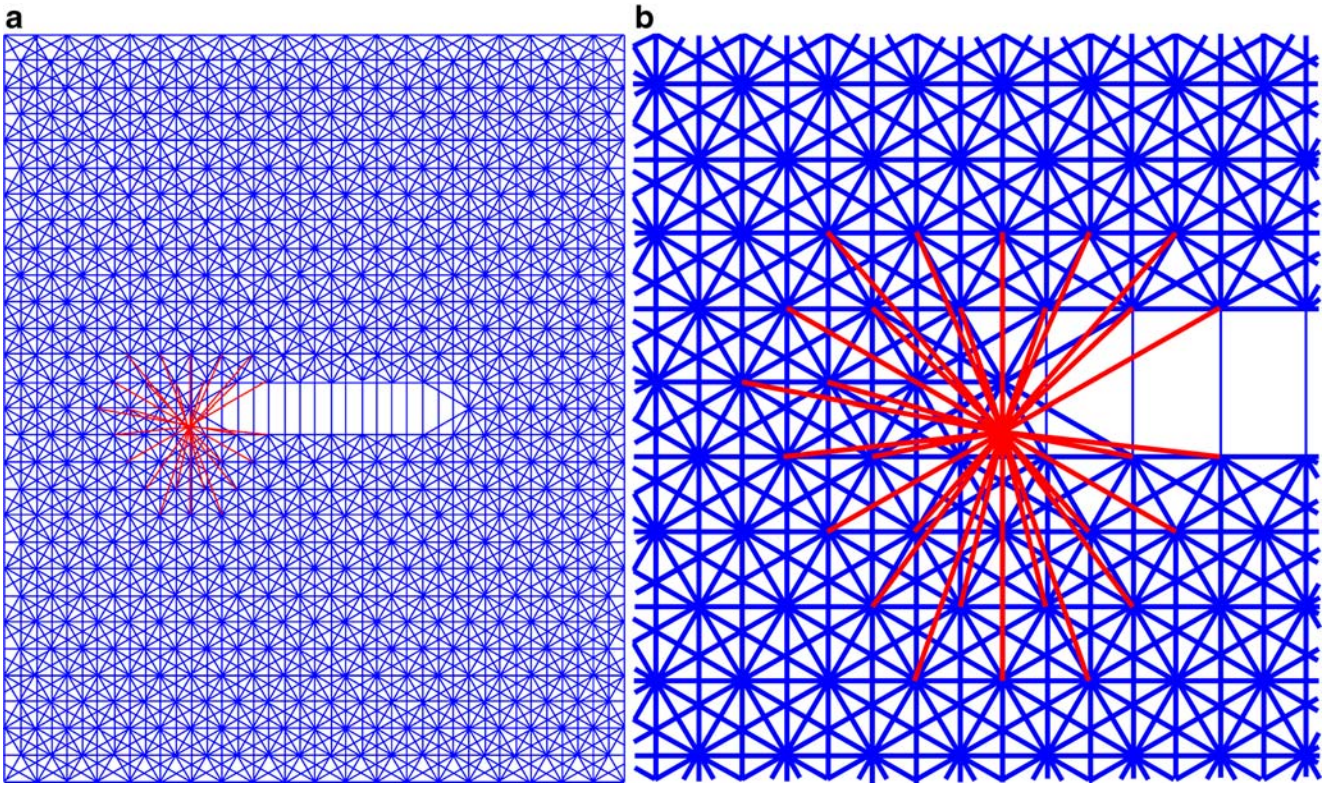

Fig. 1 Two-dimensional (2D) hexagonal iron-lattice structure (**a**) and enlarged region with one hydrogen atom embedded (**b**)

Fe potential converges smoothly to zero. The H–Fe potential has a significantly longer range of interaction; it converges to zero at about x_c=3.1, and this distance was chosen as a cut-off limit for the H–Fe interaction; H–H interactions were neglected.

The interatomic force law corresponding to the above potential is $F(R_{ij})=d\Phi(R_{ij})/dR_{ij}$. Figure 1 shows the interatomic bonds in a two-dimensional (2D) hexagonal iron-lattice structure with a nano-scale crack (Fig. 1a) and an enlarged region near the crack tip (Fig. 1b) containing the embedded hydrogen atom. In this figure the blue lines illustrate the iron–iron interaction and the red lines the hydrogen–iron interaction.

In the following, both load and displacement boundary conditions are considered for the structure. Within the framework of the MS approach, an inelastic deformation of the iron structure is considered as a sequence of constrained equilibrium states. The load/displacement is applied incrementally to the outmost atoms and the system is then allowed to relax to its equilibrium configuration. The search for a current equilibrium state is performed by an iterative procedure where, at each step, the atomic system is treated as a truss-type structure. In the context of structural mechanics, a link between any two interacting atoms can be considered as a two-node element with two degrees of freedom at each node for the planar case and with three degrees for the three-dimensional (3D) case.

The stiffness of such an element mathematically constitutes the second derivative of the potential energy function:

$$[\mathbf{k_0}] = \ddot{\Phi}(R_{ij}) \cdot \begin{bmatrix} 1 & -1 \\ -1 & 1 \end{bmatrix} \tag{4}$$

The modified Morse potential is a highly non-linear function, which switches the sign of its second derivative from positive to negative at the interatomic distance at which the interaction force reaches the maximum.

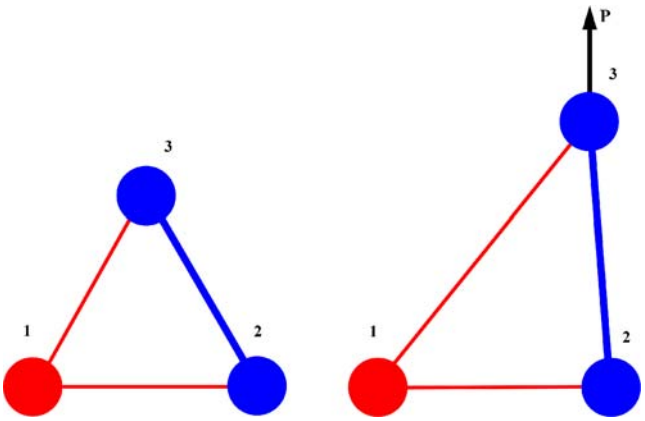

Fig. 2 Test problem: **a** 3-atom structure—initial configuration; **b** structure under the load—new equilibrium state (computed)

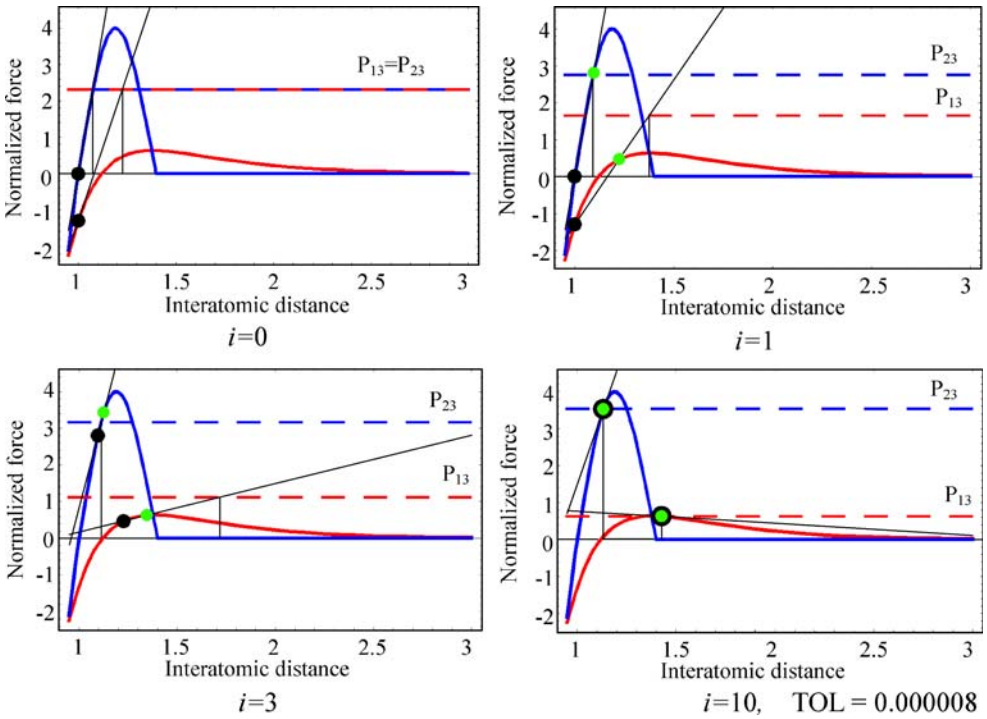

Fig. 3 Search for solution. *Black points* Search results after the (*i*−1)th iteration, *green points* iterations after the *i*th iteration, *dashed horizontal lines* projections of the external load on the direction of the link 1–3 (*dashed red line*) and link 2–3 (*dashed blue line*)

In the global coordinate system, the element stiffness matrix $[k_{el}]$ is

$$[\mathbf{k_{el}}] = [\mathbf{T}_\varphi]^{\mathbf{T}}[\mathbf{k}_0][\mathbf{T}_\varphi] \tag{5}$$

where $[T_\varphi]$ is a coordinate transformation matrix. For a plane truss element (2D-structure)

$$[\mathbf{T}_\varphi]_{2\times4} = \begin{bmatrix} \cos\varphi & \sin\varphi & 0 & 0 \\ 0 & 0 & \cos\varphi & \sin\varphi \end{bmatrix} \tag{6}$$

where φ is the angle between the x-axis in the local coordinate system and the x-axis in the global one. The operation (5), (6) produces a 4×4-matrix.

For a space truss element (3D-structure)

$$[\mathbf{T}_\varphi]_{2\times6} = \begin{bmatrix} l_1 & m_1 & n_1 & 0 & 0 & 0 \\ 0 & 0 & 0 & l_1 & m_1 & n_1 \end{bmatrix} \tag{7}$$

where l_1, m_1 and n_1 are direction cosines of the element axis. In this case $[k_{el}]$ is a 6×6 matrix.

After assembling the elements, the equilibrium state of the crystal is described by the following nonlinear algebraic system of equations

$$[\mathbf{K}]\{\mathbf{D}\}=\{\mathbf{R}\}_A \tag{8}$$

where **[K]** is the structure stiffness matrix, which is a function of displacements and thus varies at each iterative step; **{D}** is the nodal displacement vector; and $\{\mathbf{R}\}_A$ is the force vector.

The solution of such a system, namely the search for a displacement vector for a given load, requires the use of an appropriate incremental/iterative procedure. Based on the analysis performed, the Inverse Broyden's Algorithm (IBA) [23, 24], which belongs to the class of quasi-Newton methods, was selected as the method of choice for the simulation. Further implementation showed that it can handle the problem of high non-linearity including the positive-to-negative transition of element stiffness.

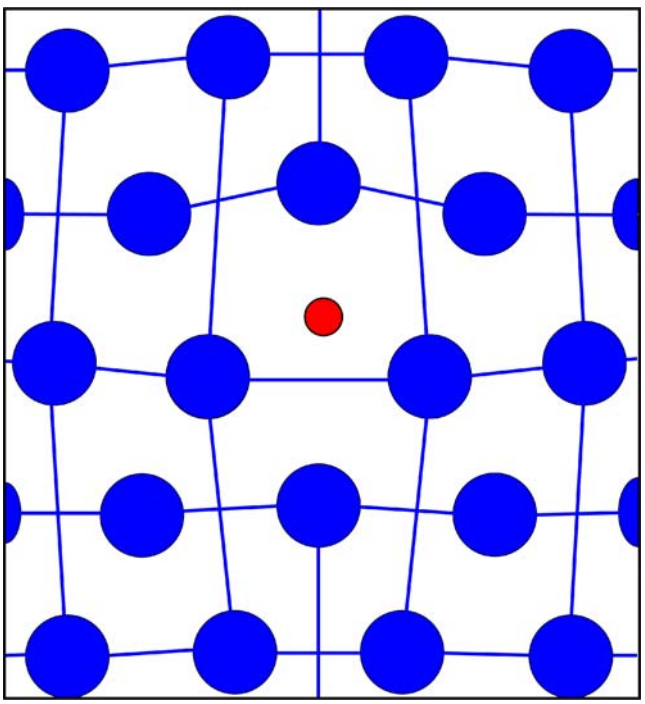

Fig. 4 Relaxed 2D hexagonal iron structure with one hydrogen atom (*red*) embedded

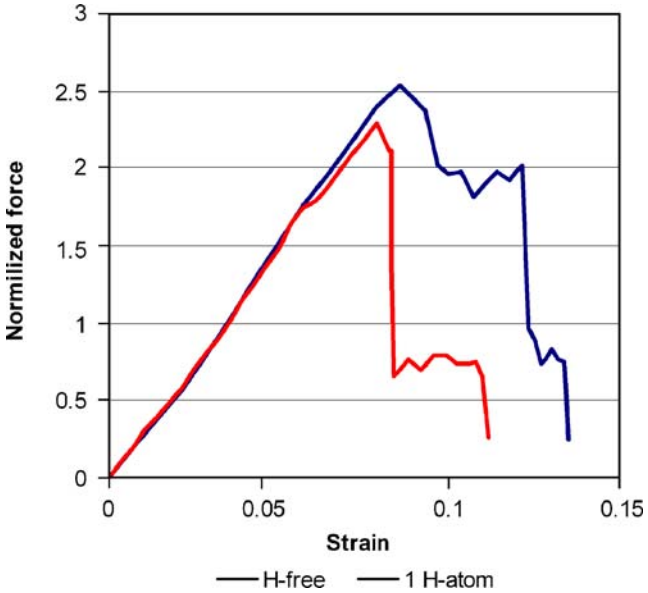

Fig. 5 Force-strain curves for a hydrogen-free sample and a sample with one H-atom embedded

The IBA represents the generalization of the Secant method extended to systems of nonlinear equations. The important feature of the IBA method is that it deals with the updating of the inverse of the global stiffness matrix and not with the stiffness matrix itself.

For the *i*-th iteration we can write [23]

$$[\mathbf{K}]_{i-1}\{\Delta\mathbf{D}\}_i=\{\Delta\mathbf{R}\}_{i-1} \tag{9}$$

$$[\mathbf{K}]_i\{\Delta\mathbf{D}\}_i=-\{\mathbf{y}\}_i \tag{10}$$

where $\{\Delta\mathbf{D}\}_i=\{\mathbf{D}\}_i-\{\mathbf{D}\}_{i-1}$ is the displacement increment; $\{\Delta\mathbf{R}\}_{i-1}=\{\mathbf{R}\}_A-\{\mathbf{R}\}_{i-1}$ is the load imbalance; $\{\mathbf{y}\}_i=\{\Delta\mathbf{R}\}_i-\{\Delta\mathbf{R}\}_{i-1}$ is introduced to simplify Eq. 10, $[\mathbf{K}]_i$ can be regarded as a secant-stiffness matrix, and *i* is the iteration number.

From Eqs. 9 and 10 we can find $[\mathbf{K}]_i$ by making a minor change to $[\mathbf{K}]_{i-1}$ consistent with the secant condition Eq. 10:

$$[\mathbf{K}]_i^{-1}=[\mathbf{K}]_{i-1}^{-1}+\left(\{\Delta\mathbf{D}\}_{i-1}-[\mathbf{K}]_{i-1}^{-1}\{\mathbf{y}\}_{i-1}\right)\{\mathbf{v}\}_{i-1}^{\mathrm{T}}, \tag{11}$$

where $\{\mathbf{v}\}_{i-1}^{\mathrm{T}}\{\mathbf{y}\}_{i-1}=1$

When the following expressions are defined,the method is called the Broyden's Good Method (BGM) [24]

$$\{\mathbf{v}\}_i=\frac{\left([\mathbf{K}]_i^{-1}\right)^T\{\Delta\mathbf{D}\}_i}{\{\Delta\mathbf{D}\}_i^T[\mathbf{K}]_i^{-1}\{\mathbf{y}\}_i},\quad \{\Delta\mathbf{D}\}_i^T[\mathbf{K}]_i^{-1}\{\mathbf{y}\}_i\neq 0 \tag{12}$$

Applying the Sherman and Morrison formula [24, 25], and denoting $[\mathbf{Z}]=[\mathbf{K}]^{-1}$, we obtain the following expression for the stiffness matrix at the *i*th iteration

$$[\mathbf{Z}]_i=[\mathbf{Z}]_{i-1}+\frac{\left(\{\Delta\mathbf{D}\}_i-[\mathbf{Z}]_{i-1}\{\mathbf{y}\}_i\right)\{\Delta\mathbf{D}\}_i^T[\mathbf{Z}]_{i-1}}{\{\Delta\mathbf{D}\}_i^T[\mathbf{Z}]_{i-1}\{\mathbf{y}\}_i} \tag{13}$$

As one can see, the above computation involves only matrix multiplication at each step and, as such, requires $\boldsymbol{O}(N^2)$ arithmetic calculations. The calculation of $[\mathbf{K}]_i$ is therefore bypassed and this is a considerable improvement compared with the Newton's method where we need $\boldsymbol{O}(N^3)$ arithmetic operations to solve the linear system. To start the procedure we need an initial approximation, $[\mathbf{K}]_0$, and its inverse $[\mathbf{Z}]_0$. Then, at each iteration, $[\mathbf{Z}]_0$ is improved by the addition of a matrix update, expressed by the second term in Eq. 13. This requires storage of the inverse matrix, which, for modern computers, does not constitute a serious problem.

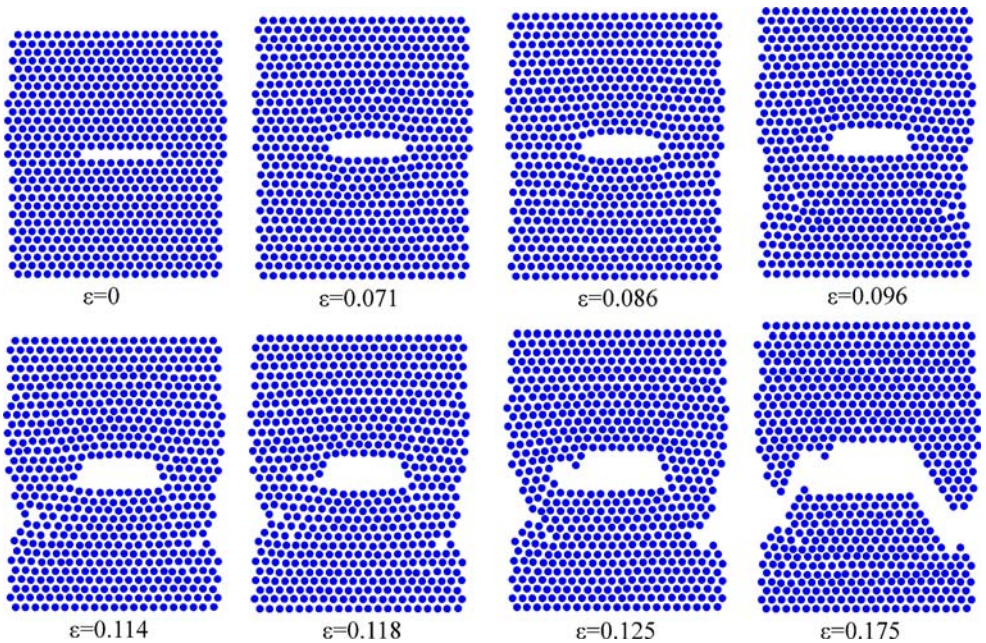

Fig. 6 Evolution of hydrogen-free 2D iron structure

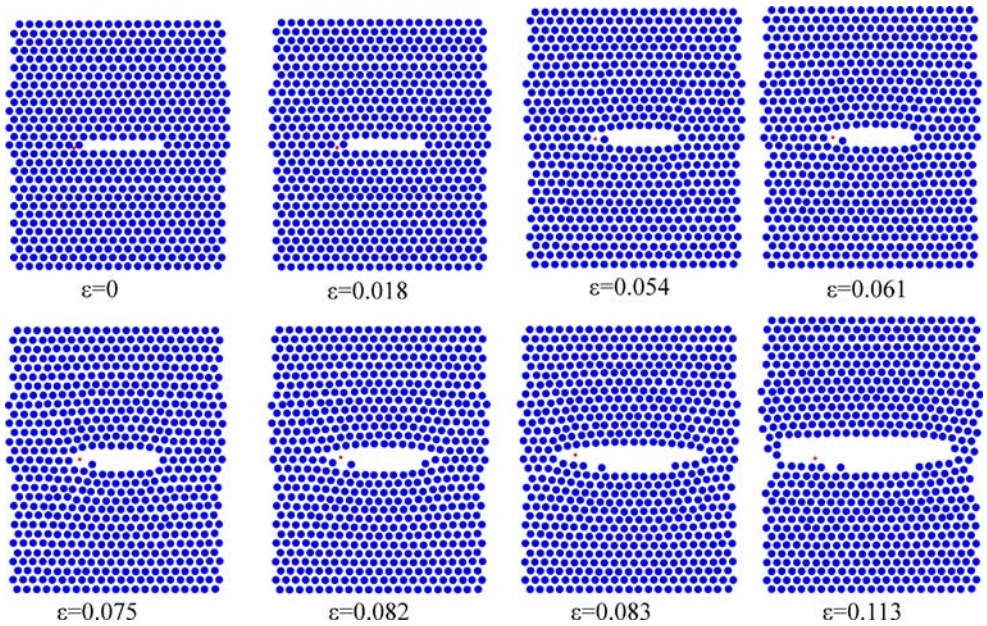

Fig. 7 Evolution of 2D iron structure with one atom of hydrogen

The above procedure was implemented in Mathematica 5.2 software. In order to illustrate how the IBA can handle the problem of high non-linearity with the positive-to-negative transition of element stiffness, the developed computer code was applied to a simple 3-node (atoms) structure (Fig. 2a).

Atom 1 simulated the imperfection (H-atom), and the laws of interaction for links 1–2 and 1–3 (Fig. 3, red line) were taken as being weaker compared with the 2–3 link (Fig. 3, blue line). The two lower nodes (atoms 1, 2) in this test structure were fully constrained, and the external load P was applied to the unconstrained top node (atom 3).

The search for a solution in the case of a 3-atom test structure is shown in Fig. 3. The four snapshots presented correspond to iterations 0, 1, 2, 10. As a zero estimate of $[\mathbf{K}]_0$, the stiffness matrix of the initial structure (Fig. 3, i=0) was used.

In the process of computing the top node (atom 3) moves and thus these lines change their positions. The adapted termination criterion for an iterative process was that recommended in [25]. We defined

$$\mathrm{CNORM} = \left(\sum \Delta D_j^2\right)^{1/2} \left(\sum D_j^2\right)^{-1/2} \tag{14a}$$

$$\mathrm{RNORM} = \left(\sum \Delta R_j^2\right)^{1/2} \left(\sum R_j^2\right)^{-1/2} \tag{14b}$$

where ΔD_j, D_j, ΔR_{i-1} and R_{i-1} denote the displacement increment, increment, load increment, and load, respectively;

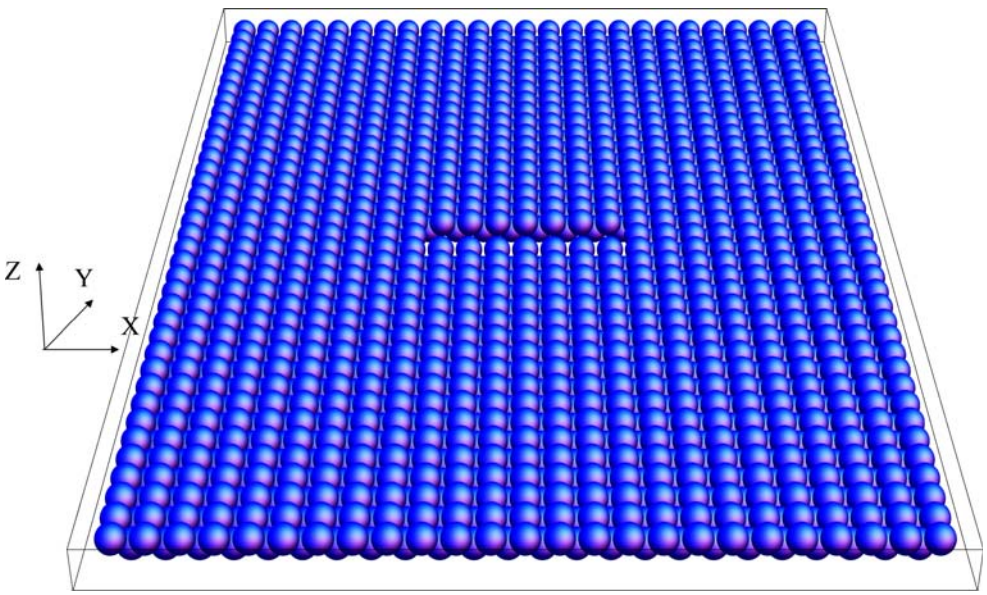

Fig. 8 3D computational cell with embedded nano-crack

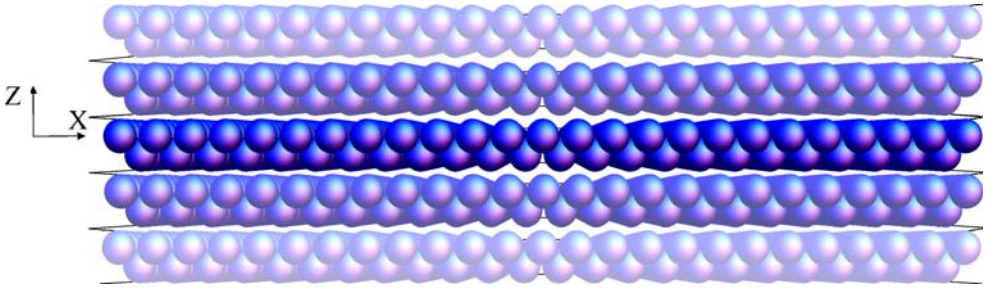

Fig. 9 Scheme of periodic–periodic boundary imposed along the *z*-direction

CNORM and RNORM are the ratios of Euclidean norms. The process is terminated when **max**(CNORM, RNORM) ≤ TOL, where TOL was chosen to be TOL=10^{-5}. The test problem terminates after the 10th iteration (Fig. 3). The final configuration of the structure is shown in Fig. 2b. The error of computing of internal forces applied to the top node (atom 3) was 1.024×10^{-4}%.

Results and discussion

2D structure

According to present knowledge, the accumulation of hydrogen in a subvolume located in the vicinity of a crack tip plays a critical role in hydrogen-enhanced fracture [26]. A 2D hexagonal structure with 623 atoms of iron and an identical structure with one hydrogen atom embedded were used to estimate the effect of hydrogen on the process of cracking. Figure 1a illustrates the computational cell containing the central crack and one hydrogen atom. In this figure the blue lines illustrate the iron–iron interaction and the red lines the hydrogen–iron interaction.

After inserting the hydrogen atoms, and before applying the external loading, the system was relaxed by quasi-Newton method in a few steps. The initial relaxation was performed for the weakened hydrogen–iron interatomic forces. The final relaxed configuration was obtained by incrementally increasing this force and applying the relaxation procedure after each increment. This approach was used to avoid numerical instability of the solution. The reason for this problem is that the direct insertion of hydrogen atoms often leads to inappropriately close distances between the hydrogen and the neighboring iron atoms, thus causing extremely high repulsive interatomic forces, which result in numerical instability and collapse of the solution.

Figure 4 shows the 2D hexagonal iron structure with one hydrogen atom after the relaxation procedure, where the H-atom is denoted in red. As can be seen, the hydrogen atom pushes apart the neighboring iron atoms, causing distortion of the lattice.

After insertion of a hydrogen atom into the lattice and relaxing it, the hydrogen-free sample and a sample with one hydrogen atom were both subjected to a numerical tensile test. The lower row of atoms was held fixed while the top boundary atoms were displaced upwards. Atoms belonging to the lateral edges of sample were considered to be unconstrained.

Simulation results demonstrated that the insertion of one atom of hydrogen in the vicinity of a crack tip caused a 9.7% loss in the residual strength of the numerically tested

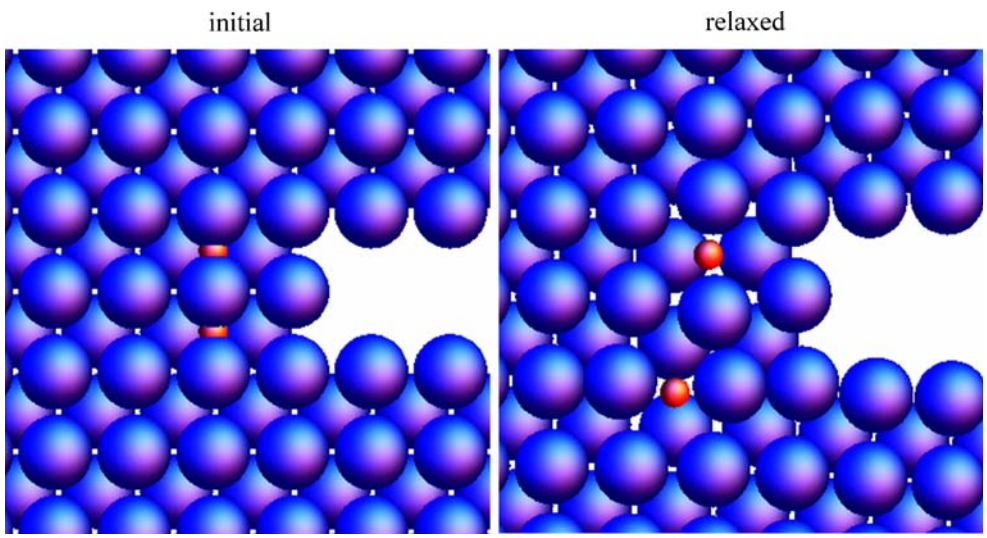

Fig. 10 Initial (unrelaxed) and final (relaxed) conurations of atoms near the crack tip

sample in comparison with the critical stress for the hydrogen-free structure (Fig. 5). The evolution of samples under tensile load is shown in Figs. 6 and 7. The results obtained allow the effect of hydrogen insertion into the 2D hexagonal structure to be qualified as embrittlement.

3D structure

In the second example, the IBA was applied to a 3D bcc iron lattice with the mode I crack embedded into the structure (Fig. 8). The chosen computation cell was 24 lattice parameters in width and 36 lattice parameters in height. A periodic boundary condition was imposed along the *z*-direction to simulate plane strain conditions (Fig. 9). A single crystal was composed of {001} planes, and the crack plane (010) was chosen from the analysis performed in [15] to facilitate an easier brittle cleavage, so that the most dangerous case would be considered. The central finite-length nano-crack was obtained by removal of a monolayer of iron atoms so that the crack had as sharp a tip as possible.

Insertion of hydrogen atoms into the 3D bcc iron lattice was performed in a few steps in the same manner as for the 2D case. We started with the weakened hydrogen–iron interatomic forces and incrementally increased this force, applying a relaxation procedure after each increment until the final relaxed configuration was obtained.

It was found that, after relaxation, the hydrogen atoms moved to octahedral interstitial sites, in accordance with Olander's assumptions concerning the behavior of hydrogen in bcc iron lattice [9]. Upon being inserted into some octahedral interstitial site, the atom of hydrogen can jump into another interstitial site after relaxation. Figure 10 illustrates the initial (unrelaxed) and final (relaxed) configura-

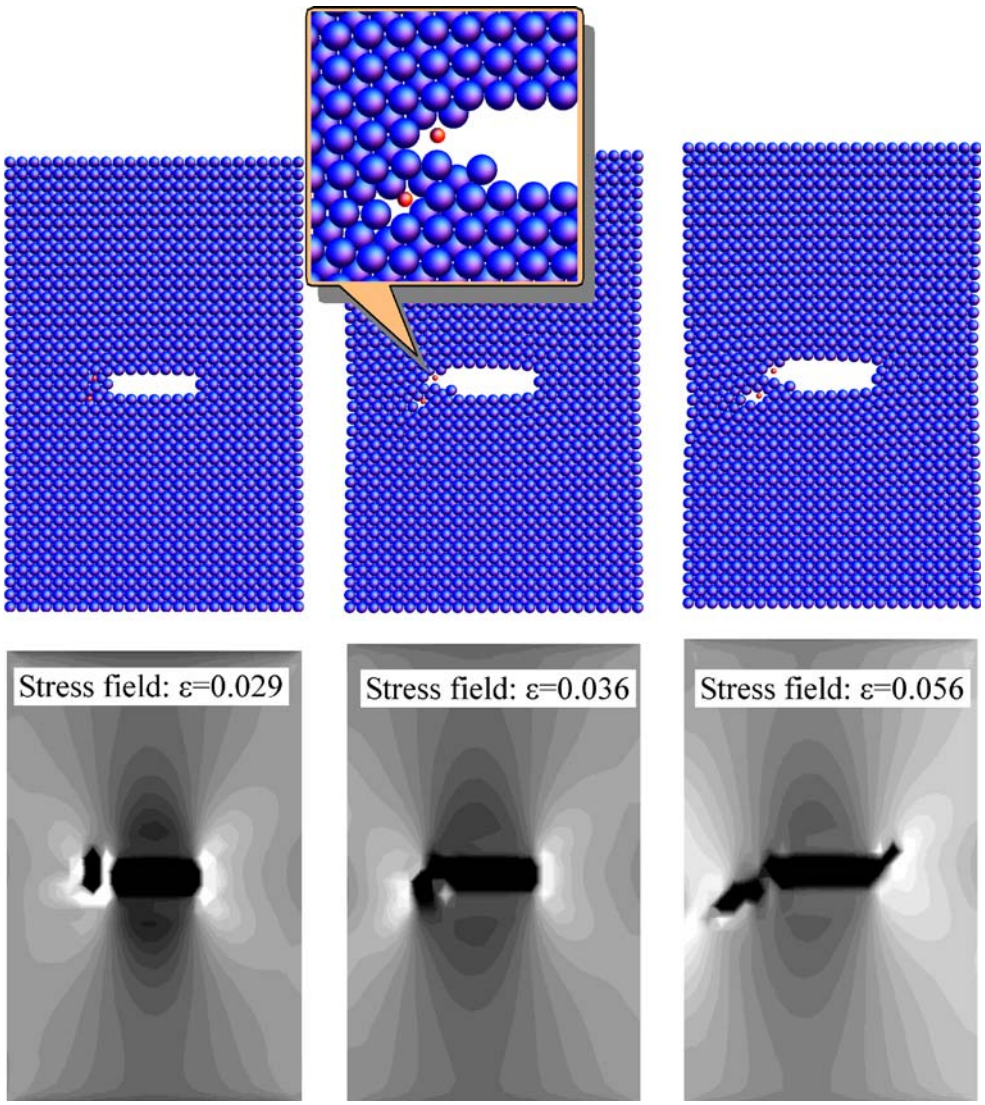

Fig. 11 Nano-voids nucleation and coalescence. *Upper panels* Stress field patterns, *lower panels* evolution of the stress field patterns. *White* and *black* denote the highest and the lowest levels of stress intensity, respectively

tion of two hydrogen atoms near the crack tip. This is a 2D projection of a 3D computation cell in a (001) plane and it shows two atomic layers.

One can see the transition of one H-atom from the initial interstitial site into another interstitial site. The other H-atom shown in Fig. 10 remained at the same interstitial sites after relaxation. Since the periodic boundary conditions and plane strain state were considered, each H-atom in fact represented an infinite string of hydrogen atoms placed at interstitial sites along the [001] line.

Once the initial relaxation has been completed, the constant displacement increments were applied to all atoms in the upper plane in order to simulate a uniaxial tensile loading in the *y*-direction. The lower plane of the sample was held fixed while the vertical boundaries were considered to be free surfaces. After each incremental displacement, the structure was relaxed to an equilibrium configuration using the MS method, so that fracture simulation was interpreted as a series of equilibrium states corresponding to the history of external load/displacement applied to the structure. The results of the simulation are shown in Fig. 11; this figure illustrates the three stages of structure evolution, where each frame corresponds to a particular strain level ranging from 0.029 to 0.056.

The black and white pictures in Fig. 11 (lower panels) illustrate the evolution of the stress field pattern within the structure during the simulation run. In these pictures we can observe zones of low stress under and above the crack and zones of high stress formed near the crack tip. We find that examining the local stress distribution is the most practical way to detect defect nucleation and to visualize the future growth path of the crack.

Stress field patterns (Fig. 11) serve to provide an understanding of the phenomenon of hydrogen-assisted cracking (in a mechanistic sense). The structural properties of the crystal are affected by the type of potential functions chosen to describe the H–Fe and Fe–Fe interatomic interactions. The Olander Fe–H potential has a longer equilibrium distance compared with the Fe–Fe potential. Because of the repulsive constituent of the Olander potential, the hydrogen atom pushes away the neighboring iron atoms and causes a severe distortion of the lattice. This lattice distortion leads to serious weakness of iron–iron bonds in the vicinity of the hydrogen atom and to the nucleation of nano-voids under the applied load. After further loading, these nano-voids can coalesce and eventually form a crack (Fig. 11).

One can see that linking with voids causes the crack tip to make a big jump and, when that happens, the highest stress concentration moves to the area adjacent to the new position of the crack tip (Fig. 11). In the process of voids and crack coalescence, the hydrogen atom leaves the lattice and moves to the cleavage space (Fig. 11). According to [12], this phenomenon has been observed experimentally. Thus the presence of the atomic hydrogen near the crack tip leads to decohesion of bcc iron; the corresponding effect is called embrittlement. Further tensile loading ultimately results in material degradation. Calculations have shown that the presence of one and two atoms of hydrogen in the area near the crack tip caused losses of 14.1% and 22%, respectively, in the residual strength of the numerically tested samples compared with the critical stress for the hydrogen-free material; further increases in the number of H-atoms did not lead to a significant loss of strength.

Conclusions

We have performed an MS simulation of hydrogen-assisted cracking in 2D hexagonal and 3D bcc iron structures under tensile loading. The Morse potential function developed by Olander [9], and the modified Morse potential developed by Fujiwara and Ishii [21] were used to describe the H–Fe and the Fe–Fe interatomic interactions, respectively. The atomic system was treated as a truss-type structure. It is shown that the quasi-Newton method allows computationally efficient analysis of highly non-linear lattice structures with imperfections. Simulation results demonstrated a strong effect of hydrogen on the mechanisms of deformation and crack propagation in iron crystal. In other words, the computer simulation showed that the presence of the atomic hydrogen near the crack tip leads to severe distortion of the iron lattice, structural decohesion and a loss of strength in comparison with the hydrogen-free sample.

References

1. Wang J, Vehoff H (1991) Scripta Metall 25:1339–1344
2. Kimura A, Birnbaum HK (1990) Acta Metall Mater 38:1343–1348
3. Evaluation of hydrogen embrittlement of SAFKEG 3940A Package in KAMS WSRC-TR-2003–00196, US Department of Energy, 2003
4. Interrante CG (1982) Basic aspects of the problems of hydrogen in steels. ASM, Washington DC, pp 3–16
5. Gehlen PC, Markworth AJ, Kahn LR (1976) Nucl Metall 20 (2):689–694
6. Markworth AJ, Kahn LR, Gehlen PC, Hahn GT (1981) Res Mech 2:141–162
7. Beeler JR (1988) Atomistic computer experiments. In: Arsenault RJ, Beeler JR, Esterling DM (eds) Computer simulation in material science. ASM, Washington DC, pp 45–78
8. Johnson RA (1966) Phys Rev 145:423–433
9. Olander DR (1971) J Phys Chem Solids 32:2499–2516
10. McCoy JK, Markworh AJ (1985) ASME PVP 99:195–209
11. Mullins M (1984) Acta Metall 32:381–388
12. Hu Z et al (1999) Modell Simul Mater Sci Eng 7:541–551
13. Daw MS, Baskes MI (1983) Phys Rev Lett 50:1285–1288

14. Hu SY, Ludwig M, Kizler P, Schmauder S (1998) Modell Simul Mater Sci Eng 6:567–586
15. Kohlhoff S, Gumbsch P, Fischmeister HF (1991) Philos Mag A 4:851–878
16. Saraev D, Kizler P, Schmauder S (1999) Simul Mater Sci Eng 7 (6):1013–1023
17. Shastry V, Farkas D (1996) Modell Simul Mater Sci Eng 4:473–492
18. Burden RL, Faires JD (1985) Numerical analysis. Prindle, Veber and Schmidt, Boston
19. Leach AR (2001) Molecular modelling: principles and applications. Prentice Hall, Pearson Education, Harlow, UK
20. Press WH et al (1992) Numerical recipes: the art of scientific computing. Cambridge University Press, Cambridge
21. Fujiwara T, Ishii Y (1980) J Phys F: Met Phys 10:1901–1911
22. Girilfalco LA, Weizer VG (1959) Phys Rev 114:687–690
23. Broyden CG, Dennis JE Jr, Mor'e JJ (1973) J Inst Math Appl 12:223–245
24. Martínez JM (2000) J Comput Appl Math 124(1–2):97–122
25. Cook RD, Plesha ME (1989) Concepts and applications of finite element analysis. Wiley, New York
26. Perng TP, Altstetter CJ (1986) Modeling of temperature dependent cracking of stainless steels. In: Modeling environmental effects on crack growth process. Metallurgical Society, pp 273–299